

## Structural analysis of a (Pt/Co)<sub>3</sub>/IrMn multilayer: Investigation of sub-nanometric layers by tomographic atom probe

R. Lardé,<sup>1</sup> L. Lechevallier,<sup>1,a)</sup> A. Zarefy,<sup>1</sup> A. Bostel,<sup>1</sup> J. Juraszek,<sup>1</sup> J. M. Le Breton,<sup>1</sup> B. Rodmacq,<sup>2</sup> and B. Dieny<sup>2</sup>

<sup>1</sup>Groupe de Physique des Matériaux, UMR CNRS 6634, Université de Rouen, Avenue de l'Université, BP 12, 76801 Saint Etienne du Rouvray, France

<sup>2</sup>SPINTEC (URA 2512 CNRS/CEA), INAC, CEA/Grenoble, 17 Avenue des Martyrs, 38054 Grenoble, France

(Received 8 December 2008; accepted 22 February 2009; published online 22 April 2009)

The structure of a Ta<sub>3 nm</sub>/[(Pt<sub>2 nm</sub>/Co<sub>0.4 nm</sub>)<sub>3</sub>/IrMn<sub>7 nm</sub>]/Pt<sub>10 nm</sub> multilayer exhibiting perpendicular exchange bias has been investigated by x-ray reflectometry and laser-assisted tomographic atom probe (LATAP). A strong intermixing at the Co/IrMn interface is pointed out by x-ray reflectometry, this interface being more diffuse than the IrMn/Pt interface. A direct observation of this intermixing at the atomic scale is obtained thanks to the LATAP in real space. The three-dimensional reconstructions reveal the atomic planes in the Pt layers and the Pt-Co intermixing in the (Pt/Co)<sub>3</sub> multilayer. The analysis of the concentration profiles allows to determine the chemical composition of the Co subnanometric layers; thus providing for the first time an accurate structural characterization of such layers leading to an estimation of their thickness, roughness, atomic concentration and width of their interfaces. © 2009 American Institute of Physics. [DOI: 10.1063/1.3106636]

### I. INTRODUCTION

When a ferromagnetic (FM) layer in contact with an antiferromagnetic (AFM) layer is field cooled from above the blocking temperature of the AFM layer, the hysteresis loop exhibits a shift from the zero field axis (denoted as  $H_E$ ) and an enhancement in its coercivity ( $H_C$ ) due to exchange coupling at the AFM/FM interface.<sup>1</sup> This phenomenon, discovered in 1956 by Meiklejohn and Bean<sup>2</sup> and called the exchange-bias effect has been extensively studied during the past decades due to its applications in the development of spin electronic devices, such as spin valves and tunnel junctions.<sup>3,4</sup> Exchange bias was first discovered in FM/AFM bilayers with in-plane magnetic anisotropy.<sup>1</sup> A few years ago, perpendicular exchange bias was also observed in multilayers with out-of-plane magnetic anisotropy.<sup>5-7</sup> Such systems, with perpendicular exchange bias at room temperature, offer the possibility to develop spin valves or tunnel junctions with perpendicular-to-plane magnetization.<sup>8,9</sup> Among these different systems, the (Pt/Co)<sub>n</sub> (where  $n$  is the number of repeats) multilayer exchange coupled to an IrMn layer exhibits perpendicular exchange bias at room temperature.<sup>10-13</sup> The (Pt/Co)<sub>n</sub> multilayer is used as the FM layer with out-of-plane anisotropy<sup>14,15</sup> and the IrMn layer is AFM at room temperature.<sup>16,17</sup> Exchange bias is strongly influenced by interfacial roughness and chemical intermixing at the interfaces.<sup>1</sup> Moreover, in (Pt/Co)<sub>n</sub> multilayers, the nature of interfaces plays a major role in controlling both perpendicular anisotropy and Pt magnetic polarization.<sup>18</sup>

In the (Pt<sub>2 nm</sub>/Co<sub>0.4 nm</sub>)<sub>n</sub>/IrMn<sub>7 nm</sub> multilayers considered here, the very small thickness of the layers makes structural characterization of interfaces extremely difficult. X-ray reflectometry can give information about the thickness,

chemical composition, and roughness (or interface intermixing) of the layers but it probes all the interfaces together (average value on the whole sample). Transmission electron microscopy is also widely used to characterize microstructure and composition profile across the layers but for very thin polycrystalline layers, it is very difficult to obtain enough contrast between the layers and a good characterization of the possible chemical intermixing at the interfaces. Nanoscale secondary-ion mass spectrometry (Nano SIMS) analysis also provides information, but with a resolution of about several nanometers. To overcome these problems and to investigate the (Pt/Co)<sub>3</sub>/IrMn structure at the atomic scale, the laser assisted tomographic atom probe (LATAP) has been used. This technique offers an ultrahigh spatial resolution (depth resolution  $\sim 0.1$  nm) and provides a powerful method to observe the chemical composition of the interfaces at the atomic scale.<sup>19</sup> Comparisons with other high resolution analytical microscopies can be found in Ref. 20. LATAP has already been used to characterize magnetoresistive<sup>21-23</sup> and magnetostrictive<sup>24</sup> multilayers, made up of layers of nanometric thickness. The principle of the technique is based on the ionization and the evaporation of surface atoms by electric field effect. The sample is prepared in a tip shape with a top radius less than 50 nm in order to generate a very high electric evaporation field (10–60 V/nm) at the surface of the specimen by applying to the tip a positive voltage of several kilovolts. During the analysis, a dc applied voltage added to femtosecond laser pulses leads to the evaporation of the specimen, atomic plane per atomic plane. The ions are collected by a position-sensitive detector which is used to measure the time of flight (TOF) and the impact position of each ion. TOF measurement leads to the chemical identification of each atom and

<sup>a)</sup>Electronic mail: luc.lechevallier@univ-rouen.fr.

the impact position enables the original position of each atom on the specimen surface to be determined.<sup>25</sup>

In this paper, using LATAP and x-ray reflectometry, we characterize the structure of  $\text{Ta}_{3\text{ nm}}/[(\text{Pt}_{2\text{ nm}}/\text{Co}_{0.4\text{ nm}})_3/\text{IrMn}_{7\text{ nm}}]_7/\text{Pt}_{10\text{ nm}}$  multilayer focusing on the FM/AFM interfaces which are at the origin of the exchange-bias phenomenon. The thickness and the roughness of the layers are determined on the whole thickness of the multilayer, thanks to x-ray reflectometry. The structure of the multilayer is characterized, thanks to the LATAP analysis, which allows to estimate the thickness of both individual layers and interfaces. A particular attention is devoted to the subnanometric Co layers. We show that an accurate determination of the composition profile of such very thin layers can be obtained by LATAP. We compare the results obtained with the two experimental techniques and report on both the large intermixing of the Co, Pt, Ir, and Mn elements at the Co/IrMn interface, compared to the limited intermixing at the IrMn/Pt interface.

## II. EXPERIMENTAL PROCEDURES

The  $\text{Ta}_{3\text{ nm}}/[(\text{Pt}_{2\text{ nm}}/\text{Co}_{0.4\text{ nm}})_3/\text{IrMn}_{7\text{ nm}}]_7/\text{Pt}_{10\text{ nm}}$  multilayer was deposited at room temperature by dc magnetron sputtering, using a  $5.3 \times 10^{-6}$  Pa base pressure and a 0.25 Pa Ar pressure during deposition on a prepatterned substrate consisting of an assembly of flat-topped Si (100) posts in order to perform the LATAP analysis. The silicon posts have a height of 100  $\mu\text{m}$  and an area of  $10 \times 10 \mu\text{m}^2$ . This specific substrate was obtained after patterning a Si wafer by Bosch process.<sup>26</sup> The sample was annealed at 200 °C (above the blocking temperature of the IrMn layer) for 30 min and cooled under a field of 2.4 kOe applied perpendicular to the film plane, to set the unidirectional exchange anisotropy in this direction. After deposition, the posts were picked off from the wafer, glued at the top of a thin rod with conductive epoxy glue and tip-shaped using a focused Ga ion beam (FIB).<sup>22</sup>

The layers being very thin, the (Pt/Co)<sub>3</sub>/IrMn sequence has been repeated seven times in order to obtain a specimen thick enough to allow an accurate analysis of the interfaces in undamaged regions by the Ga<sup>2+</sup> ion beam during the sharpening process of the top of the tip.

Figure 1 shows a scanning electron microscopy (SEM) image of a tip obtained after the FIB process. The seven  $(\text{Pt}_{2\text{ nm}}/\text{Co}_{0.4\text{ nm}})_3/\text{IrMn}_{7\text{ nm}}$  sequences are clearly observable at the top of the tip. The tip radius is less than 50 nm.

Prepared tips were analyzed by LATAP at 80 K in an ultrahigh vacuum chamber under a  $10^{-8}$  Pa pressure. The femtosecond laser pulsed system used was an amplified ytterbium-doped laser (Amplitude System s-pulse) with a pulse length of 350 fs. Before the analysis, tip surfaces were observed by field ion microscopy under a  $2 \times 10^{-3}$  Pa Ne pressure. These observations allow orientating tip axis approximately parallel to the flight axis of the atom probe. Details on the three-dimensional (3D)-reconstruction protocol can be found in Ref. 27.

The  $\text{Ta}_{3\text{ nm}}/[(\text{Pt}_{2\text{ nm}}/\text{Co}_{0.4\text{ nm}})_3/\text{IrMn}_{7\text{ nm}}]_7/\text{Pt}_{10\text{ nm}}$  multilayer was also deposited on Si plane substrate and char-

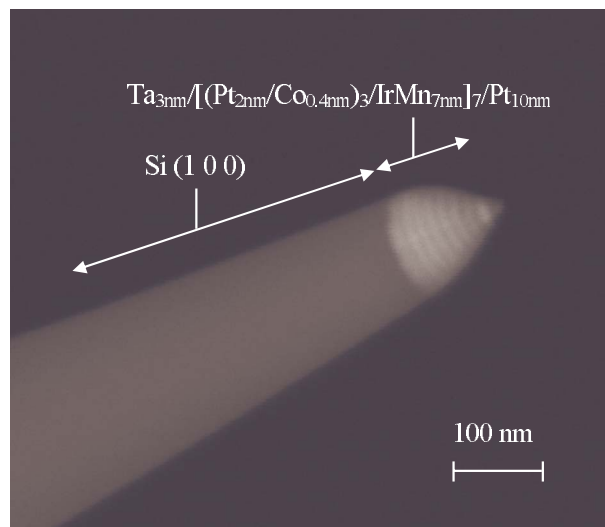


FIG. 1. (Color online) SEM of an atom probe specimen. The seven  $(\text{Pt}/\text{Co})_3/\text{IrMn}$  sequences of the  $\text{Ta}_{3\text{ nm}}/[(\text{Pt}_{2\text{ nm}}/\text{Co}_{0.4\text{ nm}})_3/\text{IrMn}_{7\text{ nm}}]_7/\text{Pt}_{10\text{ nm}}$  multilayer are revealed in the bright contrast at the top of the tip.

acterized by x-ray reflectometry, using a Bruker D8 System. The x-ray generator is equipped with a Co anticathode, using Co ( $K\alpha_1$ ) radiation ( $\lambda=0.178\ 897\ \text{nm}$ ). The obtained reflectometry curves were fitted using the SIMULREFLEC program.<sup>28</sup>

## III. RESULTS

### A. Analysis of the whole multilayer: X-ray reflectometry

Figure 2 shows the experimental and fitted x-ray reflectometry curves obtained for the whole multilayer. The experimental curve shows numerous peaks which characterize well defined layers. It has been fitted using different values for the seven  $(\text{Pt}_{2\text{ nm}}/\text{Co}_{0.4\text{ nm}})_3/\text{IrMn}_{7\text{ nm}}$  sequences. The mean values of the thickness and roughness of the different layers are given in Table I. The roughness corresponds more likely to an interfacial intermixing between two layers, but for the sake of simplicity, the roughness term has been maintained. In order to correctly identify the layers, the first Pt layer deposited on IrMn is named Pt<sub>(1)</sub>, it is followed during the deposition sequence by the Co<sub>(1)</sub>, Pt<sub>(2)</sub>, Co<sub>(2)</sub>, Pt<sub>(3)</sub>, and

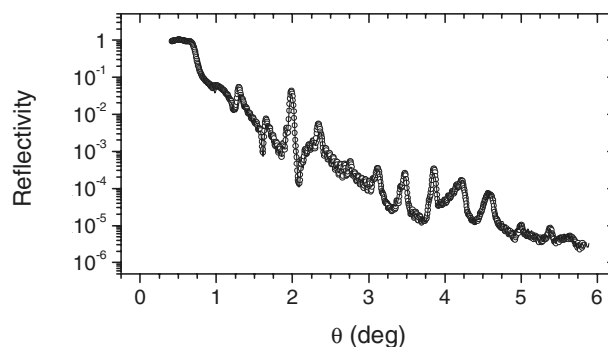


FIG. 2. X-ray reflectometry curves obtained between 0° and 6° for the  $\text{Ta}_{3\text{ nm}}/[(\text{Pt}_{2\text{ nm}}/\text{Co}_{0.4\text{ nm}})_3/\text{IrMn}_{7\text{ nm}}]_7/\text{Pt}_{10\text{ nm}}$  multilayer. The experimental and fitted curves are in open circles and continuous line, respectively.

TABLE I. Thickness and roughness of the different layers in the  $\text{Ta}_3 \text{ nm} / [(\text{Pt}_2 \text{ nm} / \text{Co}_{0.4 \text{ nm}})_3 / \text{IrMn}_7 \text{ nm}]_7 / \text{Pt}_{10 \text{ nm}}$  multilayer measured with x-ray reflectometry. The values reported for the  $(\text{Pt}/\text{Co})_3 / \text{IrMn}$  sequence correspond to the mean values obtained for the seven sequences fitted separately.

Layer	Nominal thickness (nm)	Thickness (nm $\pm$ 0.10)	Roughness (nm $\pm$ 0.10)
IrMn	7.0	6.55	0.46
Co <sub>(3)</sub>	0.4	0.23	1.18
Pt <sub>(3)</sub>	2.0	1.93	0.28
Co <sub>(2)</sub>	0.4	0.42	0.34
Pt <sub>(2)</sub>	2.0	1.97	0.48
Co <sub>(1)</sub>	0.4	0.50	0.35
Pt <sub>(1)</sub>	2.0	1.82	0.45

Co<sub>(3)</sub> layers, respectively. Thus, the IrMn layer is deposited on the Co<sub>(3)</sub> layer. The mean thicknesses of the different layers are close to the nominal values, except for the Pt<sub>(1)</sub> and Co<sub>(3)</sub> layers which are lower than the nominal values. The roughness of the different layers is between 0.28 and 0.48 nm except for the Co<sub>(3)</sub> layer which is about three times larger ( $\sim 1.2$  nm). The low thickness and the strong roughness of the Co<sub>(3)</sub> layer suggest that this layer is strongly intermixed. For both Co<sub>(1)</sub> and Co<sub>(2)</sub> layers the roughness is comparable with thickness, suggesting an intermixing between these layers and the adjacent Pt layers, which is difficult to estimate.

## B. Analysis of one sequence: LATAP

In Fig. 3 is shown the mass spectrum related to ions collected during the LATAP analysis. As expected, Mn, Co, Ir, and Pt ions are the main elements which are detected. It is worth to mention that all the peaks of the mass spectrum are clearly defined and well separated allowing accurate measurements of the atomic composition.

Figure 4 shows the spatial distribution of Mn, Ir, Pt, and Co atoms in approximately one  $(\text{Pt}_2 \text{ nm} / \text{Co}_{0.4 \text{ nm}})_3 / \text{IrMn}_7 \text{ nm}$  sequence. The reconstructed volume was oriented in order to image the interfaces in cross section, i.e., perpendicular to the plane of view. In this figure, one can observe that numerous Ir and Mn atoms are present in the  $(\text{Pt}/\text{Co})_3$  multilayer on a thickness larger than 1 nm. This shows a strong intermixing between the Co atoms of the Co<sub>(3)</sub> layer and the Ir and Mn atoms of the IrMn layer. In contrast, at the IrMn/Pt interface, Pt and Co atoms do not enter the IrMn layer. Thus the Co/IrMn interface appears to be quite diffuse, whereas the IrMn/Pt interface is much sharper. The three Co layers are clearly observed in the  $(\text{Pt}/\text{Co})_3$  multilayer. The Co<sub>(3)</sub> layer appears to be thicker than the Co<sub>(1)</sub> and Co<sub>(2)</sub> layers, as explained below. It looks like the Ir and Mn atoms have diffused through the whole Co<sub>(3)</sub> layer and were stopped by the Pt<sub>(3)</sub> layer.

The position of the Pt atoms in the  $(\text{Pt}/\text{Co})_3$  multilayer is displayed in Fig. 5. The Pt atomic planes which correspond to the Pt (111) crystalline texture are revealed in Pt<sub>(2)</sub> and Pt<sub>(3)</sub> layers deposited on Co layers. This shows that the LATAP depth resolution is better than  $\frac{1}{2}$  atomic plane, i.e.,

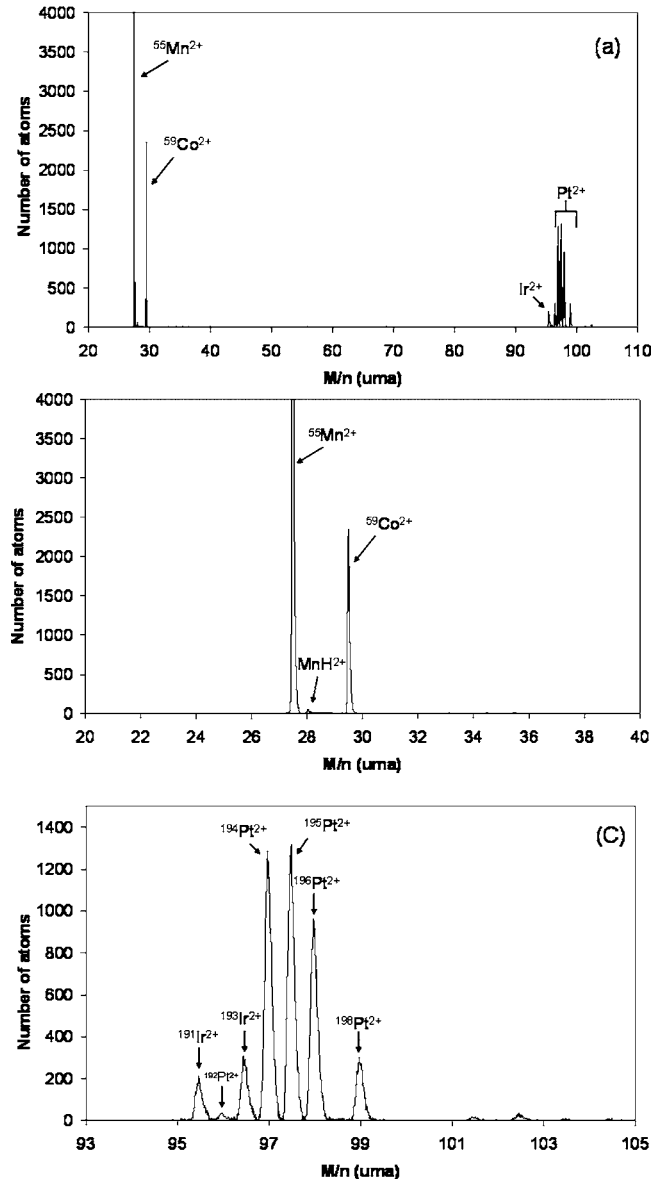


FIG. 3. Mass spectrum of the  $[(\text{Pt}_2 \text{ nm} / \text{Co}_{0.4 \text{ nm}})_3 / \text{IrMn}_7 \text{ nm}]_m$  multilayer obtained by LATAP, (a) between 20 and 110 uma showing all peaks, (b) between 20 and 40 uma to characterize the Co<sup>2+</sup> and Mn<sup>2+</sup> peaks, and (c) between 93 and 105 uma to characterize the five Pt<sup>2+</sup> peaks and two Ir<sup>2+</sup> peaks.

0.1 nm in this case. In contrast, the Pt atomic planes do not appear in the first Pt layer deposited on IrMn. It is known that the Pt (111) texture strongly depends on the buffer layer.<sup>29,30</sup> Consequently, one can deduce that the IrMn layer is not a satisfactory buffer for promoting a good (111) texture. The Co layer thus acts as a better buffer than IrMn allowing an easier growth of the Pt (111) texture.

In the fcc Pt lattice, the distance between two (111) atomic planes being equal to 0.2266 nm, we can thus estimate the thickness of the crystalline zones (see Fig. 5) to  $1.13 \pm 0.10$  and  $0.91 \pm 0.10$  nm for Pt<sub>(2)</sub> and Pt<sub>(3)</sub> layers, respectively, but also the thickness of the different layers of this system. The thickness of the Co layer between the two Pt crystalline zones is lower than 1 nm.

The concentration profiles of Pt, Co, and Mn across one  $(\text{Pt}/\text{Co})_3 / \text{IrMn}$  sequence are shown in Fig. 6. In the  $(\text{Pt}/\text{Co})_3$

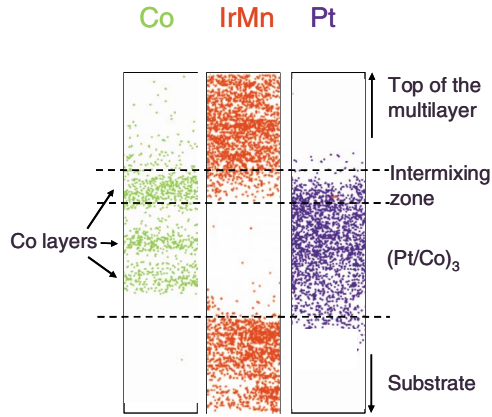


FIG. 4. (Color online) 3D reconstruction of an analyzed volume representing one sequence of the  $[(Pt_{2\text{ nm}}/Co_{0.4\text{ nm}})_3/IrMn_{7\text{ nm}}]_7$  multilayer. The spatial distribution of IrMn, Pt, and Co atoms shows the strong intermixing between the Co, IrMn, and Pt atoms at the IrMn/Co interface and the very low intermixing between Pt and IrMn atoms at the IrMn/Pt interface.

multilayer, the Pt and Co concentration profiles present maxima and minima. A Co maximum corresponds to a Pt minimum and to the center of a Co layer. According to the position of these maxima and to the shape of the distribution of Co and Pt profiles (see Fig. 6), the thickness of each layer and the thickness of the intermixing regions for each sequence were estimated.

### C. Investigation of the subnanometric Co layers

#### 1. Artifacts in the reconstruction process

The excellent depth resolution of the technique, evidenced by the observation of atomic planes in the Pt layers ( $\frac{1}{2}$  atomic plane, i.e.,  $\sim 0.1$  nm) (Fig. 5), may be slightly degraded in some regions of the specimen due to reconstruction artifacts which introduce slight depth position errors of atoms. Indeed, the difference of the evaporation fields of atoms located at the interfaces leads to local magnification effects in the reconstructed volumes which decrease the spa-

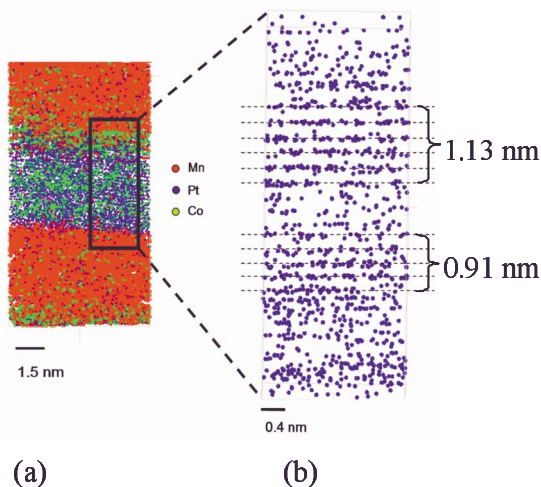


FIG. 5. (Color online) (a) 3D reconstruction of one sequence of the  $[(Pt_{2\text{ nm}}/Co_{0.4\text{ nm}})_3/IrMn_{7\text{ nm}}]_7$  multilayer showing the spatial distribution of Mn, Ir, Pt, and Co atoms. (b) Position of Pt atoms in the  $(Pt/Co)_3$  multilayer, the Pt atomic planes in the regions that correspond to the  $Pt_{(2)}$  and  $Pt_{(3)}$  layers deposited on Co layers are evidenced.

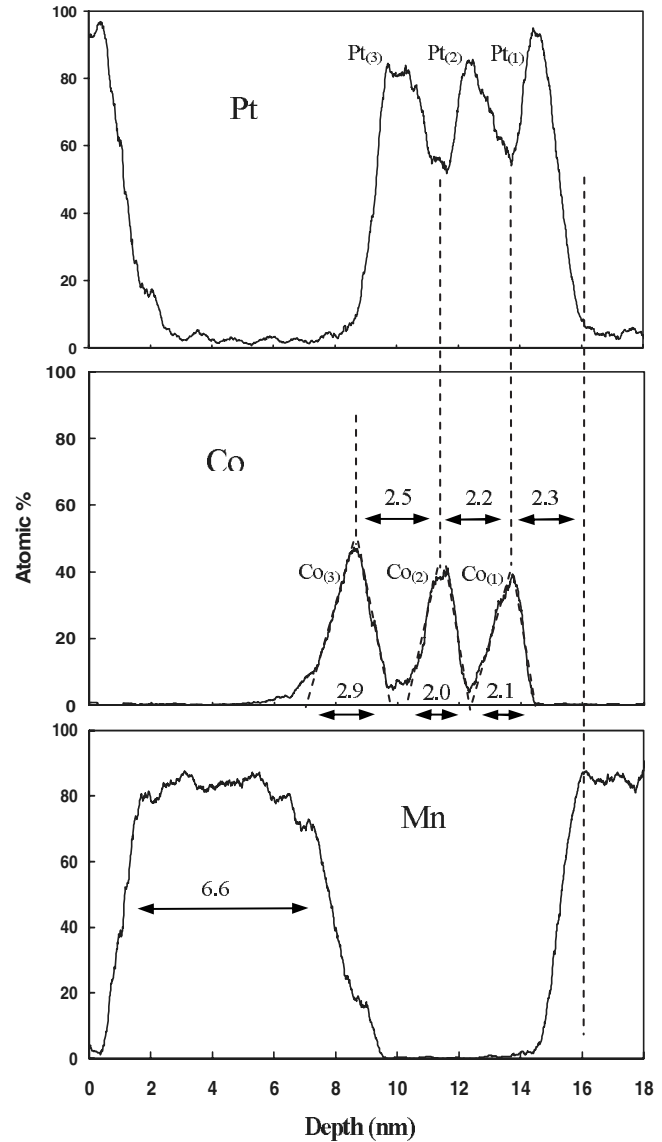


FIG. 6. Concentrations profiles of Pt, Co, and Mn atoms across the interfaces. The numerical values are in nanometers.

tial resolution. Taking into account the values of the evaporation fields of each elements (i.e.,  $E_{Ir}=53\text{ V nm}^{-1}$ ,  $E_{Mn}=30\text{ V nm}^{-1}$ ,  $E_{Pt}=48\text{ V nm}^{-1}$ , and  $E_{Co}=37\text{ V nm}^{-1}$ ),<sup>31</sup> it can be assumed that the atoms of the IrMn layer (Ir 20 at. % and Mn 80 at. %) are evaporated under a mean evaporation field  $E_{IrMn}=34.6\text{ V nm}^{-1}$  (which corresponds to a low field environment), whereas the very thin  $Co_{(1)}$  and  $Co_{(2)}$  layers being surrounded by Pt layers are evaporated under a high field environment. Due to the atom position error caused by the evaporation conditions of the Co atoms, the  $Co_{(1)}$  and  $Co_{(2)}$  layers with a 0.4 nm nominal thickness will appear thicker in the 3D-reconstructed volume. For the  $Co_{(3)}$  layer, located at the strongly intermixed Co/IrMn interface, one can consider that in the top part and in the bottom part of this layer, the evaporation fields correspond to the  $Ir_{20}Mn_{80}$  and  $Co_{20}Pt_{80}$  alloys, respectively, i.e., to the weighted averaging sum,  $E_{IrMn}=34.6\text{ V nm}^{-1}$  and  $E_{PtCo}=45.8\text{ V nm}^{-1}$ . The values of  $E_{IrMn}$  and  $E_{Co}$  evaporation fields being very close, the CoIrMn intermixing does not lead to an important modifica-

tion of the CoIrMn evaporation field. By contrast,  $E_{\text{PtCo}}$  being higher than  $E_{\text{IrMn}}$ , the CoIrMn/(Pt/Co) transition leads to an increase in the evaporation field (from 34.6 to 45.8 V nm<sup>-1</sup>). Thus, one can consider that the Co<sub>(3)</sub> layer is mainly evaporated under a low field environment, contrary to the two Co<sub>(1)</sub> and Co<sub>(2)</sub> layers which are evaporated under high field environment. Consequently, the depth calibration being realized from the Pt atomic planes (evaporated under high field), the Co<sub>(3)</sub> layer appears with a larger width and height than the ones of the Co<sub>(1)</sub> and Co<sub>(2)</sub> layers. Indeed, the difference of evaporation conditions between the Co<sub>(3)</sub> layer and the two others Co layers leads in the 3D reconstruction to a magnification  $f$  of the Co<sub>(3)</sub> layer roughly corresponding to the square of the ratio of the evaporation fields  $f \approx (E_{\text{Pt}}/E_{\text{IrMn}})^2 = (48/34.6)^2 \approx 2$ .

## 2. Artifacts in the depth concentration profiles

It is well known that the numerical sampling boxes used to calculate the depth concentration profiles and their slight misalignment relative to the interfaces causes a slight artificial enlargement of each layer.<sup>19</sup> This effect is added to the reconstruction artifacts. In the following section we propose to take into account the previous mentioned artifact sources to obtain a corrected concentration profile of the Co layers.

## 3. Calculation of corrected concentration profiles

Figure 7(a) shows the calculation principle of a Co peak representative of a 0.4 nm Co layer surrounded by two Pt layers. This peak results from two convolutions. The first one is the convolution of two rectangular functions, representing the concentration profile of a perfect and pure Co layer (height= $H$  for a 100% Co concentration and width= $2$  atomic planes  $\sim 0.4$  nm) and the depth position error (surface= $1$  and width  $\approx 2 \times 1.5$  atomic planes, i.e.,  $\sim 0.7$  nm), respectively. The second one is the convolution of the previous obtained function with a rectangular function (surface= $1$  and width= $0.5$  nm) which takes into account for the width and the misalignment of the numerical sampling box used to compute the composition. The surface of the two rectangular functions is fixed to one in order to maintain constant the total number of atoms, before and after applying the convolutions. The obtained peak presents a 1.6 nm thickness and a  $0.54H$  height, which is not consistent with the observed peaks for the Co<sub>(1)</sub> and Co<sub>(2)</sub> layers (see Fig. 6). This difference shows that Pt–Co intermixing in the Co layers has to be taken into account.

Let us consider now a Co layer intermixed with Pt atoms with a Co distribution over four atomic planes as in the Fig. 7(b). In this case, the rectangular functions corresponding to the depth position error and to the width of the numerical sampling box remain unchanged and the obtained peak is in a good agreement with the experimental data ( $0.47H$  height and 2.1 nm width) for the Co<sub>(1)</sub> and Co<sub>(2)</sub> layers.

If one have considered that the Co atoms were distributed over six atomic planes, one would have found after both convolutions a Co peak larger than the experimental one (2.6 nm instead of 2.1 nm). This suggests that the correct model

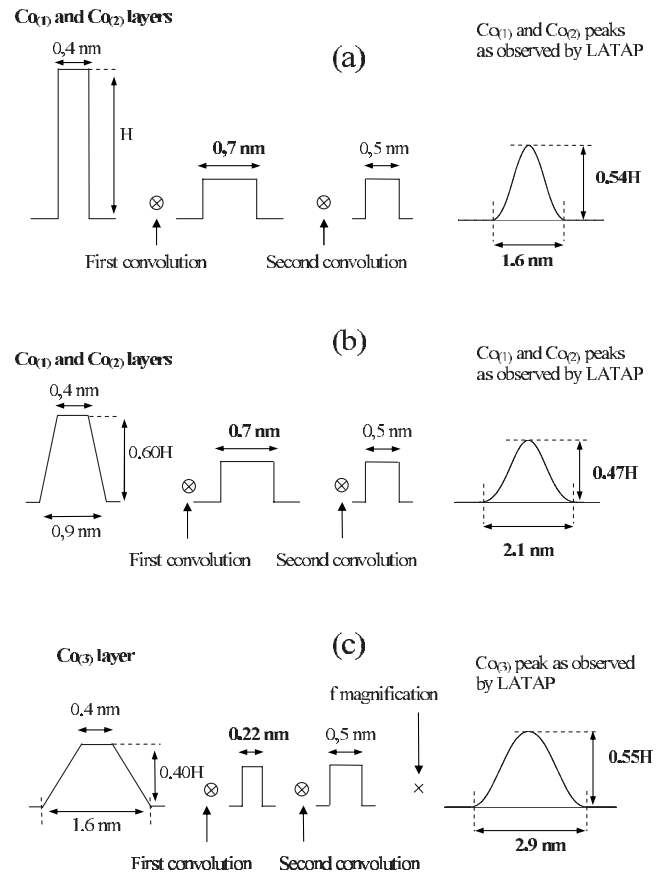


FIG. 7. Model of concentration profile of the 0.4 nm Co<sub>(1)</sub> and Co<sub>(2)</sub> layers surrounded by two Pt layers (a) with perfectly smooth interfaces and (b) with one atomic plane of Pt–Co intermixing on each side. (c) Model of concentration profile of the strongly intermixed Co<sub>(3)</sub> layer.

of the repartition of the Co atoms in the Co<sub>(1)</sub> and Co<sub>(2)</sub> layers is the one for which the Co layer extends over four atomic planes, with two Co-rich planes in the middle of the layer and sharp Co–Pt interfaces of one monolayer on each side. This result is in agreement with that obtained by Nakajima *et al.*<sup>18</sup> and Ji *et al.*<sup>32</sup> who found an intermixing of only one monolayer for each Co and Pt layer on similar samples prepared by magnetron sputtering. This result is also in agreement with the very weak roughness of Pt–Co interfaces obtained for Ar sputtering (Pt/Co)<sub>n</sub> multilayers.<sup>33</sup>

Figure 7(c) shows the calculation principle of the Co<sub>(3)</sub> layer peak. The obtained peak results from two convolutions as above. The first one is the convolution of the Co concentration profile with a rectangular function (surface= $1$  and width= $0.22$  nm) representing the depth position uncertainty. The width of this latter function is smaller ( $0.22$  nm) than in the two previous cases ( $0.7$  nm) because the depth position error due to the field difference between IrMn and Co is negligible. In other words, in the Co<sub>(3)</sub> layer, Co atoms are evaporated under their own evaporation field. The Co<sub>(3)</sub> peak is then obtained after the second convolution with the numerical sampling box and taking into account the  $f$  magnification. A satisfactory result is obtained by considering that the Co<sub>(3)</sub> layer is intermixed with Pt, Ir, and Mn atoms with a Co atom distribution over about 1.6 nm. It results that the Co atoms in the Co<sub>(3)</sub> layer are spread in an intermixed re-

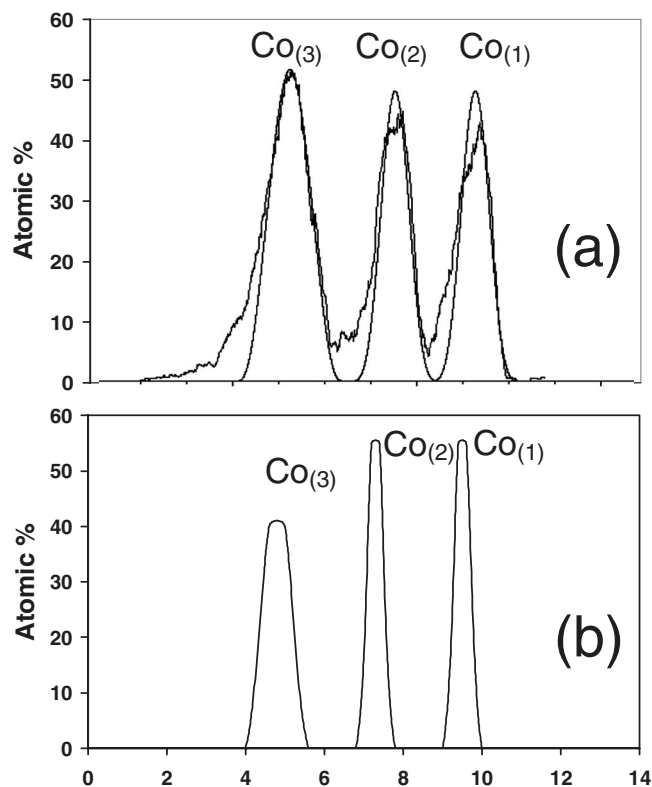


FIG. 8. (a) Fitted and experimental concentration profiles representing the three Co peaks. The fitted curve is deduced from the convolution model. (b) Repartition of the Co atoms in the three Co layers deduced from the Co modeled concentration profile.

gion approximately over seven Pt atomic planes corresponding to a 1.6 nm width. Its central part roughly contains a Co atomic concentration of about 40%.

The experimental Co concentration profile shown in Fig. 6 has been fitted according to these basic principles of concentration profile calculation. The best fittings are presented in Fig. 8(a). They were obtained by considering that the width and the height of the  $\text{Co}_{(1)}$  and  $\text{Co}_{(2)}$  layer peaks are 1.2 nm and  $0.55H$ , respectively, whereas the width and the height of the  $\text{Co}_{(3)}$  layer peak are 1.6 nm (approximately seven atomic planes) and  $0.40H$ , respectively [Fig. 8(b)].

Thus, considering the errors linked to the model and according to the concentration profiles, one can conclude that the  $\text{Co}_{(1)}$  and  $\text{Co}_{(2)}$  layers extend more likely over four to five atomic planes ( $\sim 1$  nm width) with a  $60 \pm 10\%$  Co atomic concentration in the central part. The  $\text{Co}_{(3)}$  layer extends more likely over six to eight atomic planes ( $\sim 1.6 \pm 0.2$  nm width) with a  $40\% \pm 10\%$  Co atomic concentration in the central part.

#### D. Comparison between LATAP and x-ray reflectometry results

The  $\text{Co}_{(3)}$  layer, corresponding to a strong intermixing region in which the Co atoms extend roughly over a 1.6 nm thickness, leads to a difficult estimate of the  $\text{Pt}_{(3)}$  layer thickness and roughness. As seen above, the  $\text{Co}_{(1)}$  and  $\text{Co}_{(2)}$  layers can be represented by two Co rich planes in the middle and sharp Co–Pt interfaces of about one monolayer on each side.

TABLE II. Thickness and intermixing zone of the different layers in the  $\text{Ta}_3 \text{ nm} / [(\text{Pt}_2 \text{ nm} / \text{Co}_{0.4 \text{ nm}})_3 / \text{IrMn}_7 \text{ nm}]_7 / \text{Pt}_{10 \text{ nm}}$  multilayer, deduced from the concentration profiles of the LATAP analysis. The values of the  $\text{Pt}_{(1)}$ ,  $\text{Pt}_{(2)}$ , and  $\text{Pt}_{(3)}$  layers thickness correspond to the difference between two maxima of Co peaks from which the Co–Pt intermixing can be removed to obtain the nonmixed part of the Pt layers. The thickness of the  $\text{Co}_{(1)}$  and  $\text{Co}_{(2)}$  layers corresponds to the Co layer central part (approximately two atomic planes,  $\sim 0.4$  nm) containing the higher Co amount.

Layer	Nominal thickness (nm)	Thickness (nm)	Intermixing zone (nm)
IrMn	7.0	6.6	...
$\text{Co}_{(3)}$	0.4	1.6	...
$\text{Pt}_{(3)}$	2.0	2.5	Co–Pt 0.3
$\text{Co}_{(2)}$	0.4	0.4	Pt–Co 0.3
$\text{Pt}_{(2)}$	2.0	2.2	Co–Pt 0.3
$\text{Co}_{(1)}$	0.4	0.4	Pt–Co 0.3
$\text{Pt}_{(1)}$	2.0	2.3	IrMn–Pt 0.4

This model allows estimating the thickness and the roughness of each adjacent Pt layer. Using the distances between the extrema of the Co and Pt concentration profiles (Fig. 6), the thickness and intermixing zone of the Co and Pt layers of the analyzed specimen are given in Table II.

The results of the LATAP analysis are in good agreement with the x-ray reflectometry data, except for the  $\text{Co}_{(3)}$  layer. Indeed, for this layer, x-ray reflectometry results give a higher roughness than the one of the other layers and a smaller thickness than the nominal value. This is not in contradiction with the LATAP analysis. This only reflects the fact that this layer is strongly intermixed, the diffusion of Ir and Mn in the  $\text{Co}_{(3)}$  layer being much higher than the one of Pt in Co or Co in Pt in the other layers.

The use of LATAP in the determination of the thickness and composition of subnanometric layers in materials containing different atom species, some of them with very different evaporation fields, leads to an enlargement of peaks (characteristic of each layer) in the atomic concentration profile representation. However, both the observation of Pt (111) atomic planes (which allows an accurate measurement of thicknesses) and the good knowledge of the ion trajectories and magnification due to the physics of the ion field emission allow to use a simplistic but sufficient model and to characterize the thickness, the roughness and the chemistry of a  $(\text{Pt}_2 \text{ nm} / \text{Co}_{0.4 \text{ nm}})_3 / \text{IrMn}_7 \text{ nm}$  sequence. This model also allows to determine the distribution of the atoms in the subnanometric Co layers. LATAP thus allows to directly observe in real space and chemically characterize the strong intermixing at the Co/IrMn interface which is suggested by x-ray reflectometry.

#### IV. CONCLUSION

The investigation by LATAP of a  $\text{Ta}_3 \text{ nm} / [(\text{Pt}_2 \text{ nm} / \text{Co}_{0.4 \text{ nm}})_3 / \text{IrMn}_7 \text{ nm}]_7 / \text{Pt}_{10 \text{ nm}}$  multilayer deposited at room temperature by dc magnetron sputtering allows to chemically and locally characterize the different interfaces of this multilayer and to reveal a strong intermixing at the Co/IrMn interface. By allowing a direct observation of this intermixing at the atomic scale, LATAP local and

chemical analysis reinforces the x-ray reflectometry study. We show that the Co/IrMn interface is diffuse with a strong intermixing between Ir, Mn, and Co atoms, whereas the IrMn/Pt interface is sharp.

The concentration profiles obtained thanks to LATAP reveals the subnanometric Co individual layers. The accuracy of LATAP thickness measurement when analyzing pure metals also allows to reveal the (111) atomic planes of the Pt<sub>(2)</sub> and Pt<sub>(3)</sub> layers deposited on the Co layers. A model has been realized to obtain the Co concentration profiles in the (Pt/Co) multilayer. This model takes into account both the physics of field emission and the 3D- reconstruction process when using an atom probe which gives uncertainties of the order of the Co layer thickness. This study thus provides for the first time an accurate structural characterization of these subnanometric layers leading to an estimation of their thickness, roughness, atomic concentration, and width of their interfaces.

These results show that it is necessary to take into account a large intermixing region at the Co/IrMn interface with the aim to accurately study the magnetic phenomena such as the exchange-bias effect and the perpendicular magnetic anisotropy in the (Pt/Co)<sub>3</sub>/IrMn multilayer.

## ACKNOWLEDGMENTS

The authors would like to thank F. Vurpillot and E. Cadel for numerous and useful discussions.

- <sup>1</sup>J. Nogués and I. K. Schuller, *J. Magn. Magn. Mater.* **192**, 203 (1999).
- <sup>2</sup>W. H. Meiklejohn and C. P. Bean, *Phys. Rev.* **102**, 1413 (1956).
- <sup>3</sup>B. Dieny, V. S. Speriosu, S. S. P. Parkin, B. A. Gurney, D. R. Wilhoit, and D. Mauri, *Phys. Rev. B* **43**, 1297 (1991).
- <sup>4</sup>S. Tehrani, J. M. Slaughter, M. Deherra, B. N. Engel, N. D. Rizzo, J. Slater, M. Durlam, R. W. Dave, J. Janesky, B. Butcher, K. Smith, and G. Grynkeiwich, *Proc. IEEE* **91**, 703 (2003).
- <sup>5</sup>S. Maat, K. Takano, S. S. P. Parkin, and E. E. Fullerton, *Phys. Rev. Lett.* **87**, 087202 (2001).
- <sup>6</sup>Z. Y. Liu and S. Adenwalla, *Phys. Rev. Lett.* **91**, 037207 (2003).
- <sup>7</sup>J. Sort, B. Dieny, M. Fraune, C. Koenig, F. Lunnebach, B. Beschoten, and G. Güntherodt, *Appl. Phys. Lett.* **84**, 3696 (2004).
- <sup>8</sup>C. H. Marrows, *Phys. Rev. B* **68**, 012405 (2003).
- <sup>9</sup>F. Garcia, J. Sort, B. Rodmacq, S. Auffret, and B. Dieny, *Appl. Phys. Lett.* **83**, 3537 (2003).
- <sup>10</sup>J. Sort, V. Baltz, F. Garcia, B. Rodmacq, and B. Dieny, *Phys. Rev. B* **71**, 054411 (2005).
- <sup>11</sup>S. van Dijken, J. Moritz, and J. M. D. Coey, *J. Appl. Phys.* **97**, 063907 (2005).
- <sup>12</sup>J. Sort, F. Garcia, B. Rodmacq, S. Auffret, and B. Dieny, *J. Magn. Magn. Mater.* **272–276**, 355 (2004).
- <sup>13</sup>R. F. Jiang and C. H. Lai, *J. Magn. Magn. Mater.* **272–276**, 2312 (2004).
- <sup>14</sup>P. F. Carcia, *J. Appl. Phys.* **63**, 5066 (1988).
- <sup>15</sup>B. N. Engel, C. D. England, R. A. Van Leeuwen, M. H. Wiedmann, and C. M. Falco, *Phys. Rev. Lett.* **67**, 1910 (1991).
- <sup>16</sup>H. Fuke, K. Saito, Y. Kamiguchi, H. Iwasaki, and M. Sashiki, *J. Appl. Phys.* **81**, 4004 (1997).
- <sup>17</sup>A. J. Devasahayam, P. J. Sides, and M. Kryder, *J. Appl. Phys.* **83**, 7216 (1998).
- <sup>18</sup>N. Nakajima, T. Koide, T. Shidara, H. Miyauchi, H. Fukutani, A. Fujimori, K. Iio, T. Katayama, M. Nyvlt, and Y. Suzuki, *Phys. Rev. Lett.* **81**, 5229 (1998).
- <sup>19</sup>D. Blavette, B. Deconihout, A. Bostel, J. M. Sarrau, M. Bouet, and A. Menand, *Rev. Sci. Instrum.* **64**, 2911 (1993).
- <sup>20</sup>D. Blavette, B. Deconihout, S. Chambrelaud, and A. Bostel, *Ultramicroscopy* **70**, 115 (1998).
- <sup>21</sup>X. W. Zhou, H. N. G. Wadley, R. A. Johnson, D. J. Larson, N. Tabat, A. Cerezo, A. K. Petford-Long, G. D. W. Smith, P. H. Clifton, R. L. Martens, and T. F. Kelly, *Acta Mater.* **49**, 4005 (2001).
- <sup>22</sup>D. J. Larson, A. K. Petford-Long, Y. Q. Ma, and A. Cerezo, *Acta Mater.* **52**, 2847 (2004).
- <sup>23</sup>D. J. Larson, *Thin Solid Films* **505**, 16 (2006).
- <sup>24</sup>A. Grenier, R. Lardé, E. Cadel, F. Vurpillot, J. Juraszek, J. Teillet, and N. Tiercelin, *J. Appl. Phys.* **102**, 033912 (2007).
- <sup>25</sup>B. Gault, F. Vurpillot, A. Vella, M. Gilbert, A. Menand, D. Blavette, and B. Deconihout, *Rev. Sci. Instrum.* **77**, 043705 (2006).
- <sup>26</sup>A. A. Ayon, R. Braff, C. C. Lin, H. H. Swain, and M. A. Schmidt, *J. Electrochem. Soc.* **146**, 339 (1999).
- <sup>27</sup>P. Bas, A. Bostel, B. Deconihout, and D. Blavette, *Appl. Surf. Sci.* **87–88**, 298 (1995).
- <sup>28</sup>SIMULREFLECT at <http://www-drecam.cea.fr/llb/prism/programs.html>.
- <sup>29</sup>J. Sort, B. Dieny, and J. Nogués, *Phys. Rev. B* **72**, 104412 (2005).
- <sup>30</sup>J. Kanak, T. Stobiecki, and S. Van Dijken, *IEEE Trans. Magn.* **44**, 238 (2008).
- <sup>31</sup>M. K. Miller, A. Cerezo, M. G. Hetherington, and G. D. W. Smith, *Atom Probe Field Ion Microscopy* (Clarendon, Oxford, 1996).
- <sup>32</sup>X. Ji, H. Ju, D. E. Mac Cready, and K. M. Krishnan, *J. Appl. Phys.* **98**, 116101 (2005).
- <sup>33</sup>Z. G. Li and P. F. Carcia, *J. Appl. Phys.* **71**, 844 (1992).